2013

Color Tuning of (K1−x,Nax)SrPO4:0.005Eu2+, yTb3+ Blue-Emitting Phosphors *via* Crystal Field Modulation and Energy Transfer

Pengpeng Dai
Northeast Normal University

Xintong Zhang
Northeast Normal University

Lulu Bian
Northeast Normal University

Shan Lu
Northeast Normal University

Yichun Liu
Northeast Normal University

See next page for additional authors

Journal of Materials Chemistry C

RSC Publishing

PAPER

View Article Online
View Journal | View Issue

Cite this: J. Mater. Chem. C, 2013, 1, 4570

Color tuning of $(K_{1-x},Na_x)SrPO_4$:0.005Eu^{2+}, yTb^{3+} blue-emitting phosphors *via* crystal field modulation and energy transfer†

Pengpeng Dai,[a] Xintong Zhang,*[a] Lulu Bian,[a] Shan Lu,[a] Yichun Liu[a] and Xiaojun Wang*[b]

Two series of $K_{1-x}Na_xSrPO_4$:0.005Eu^{2+} and $K_{0.4}Na_{0.6}Sr_{0.995-y}PO_4$:0.005$Eu^{2+}$, y$Tb^{3+}$ phosphors are synthesized *via* a high-temperature solid-state reaction. Their emission color can be tuned from deep blue to blue–green by modulating the crystal field strength and energy transfer. Partial substitution of K^+ with Na^+ results in a contraction and distortion of the unit cell of the $K_{1-x}Na_xSr_{0.995}PO_4$:0.005$Eu^{2+}$ host, tuning the emission from 426 to 498 nm. The red-shifted emission is attributed to an increased crystal field splitting for Eu^{2+} in a lowered symmetry crystal field. The tunable emission is further demonstrated in the cathodoluminescence spectra, which indicates that the luminescence distribution of the $K_{1-x}Na_xSr_{0.995}PO_4$:0.005$Eu^{2+}$ phosphor is very homogenous. Additionally, utilizing the principle of energy transfer, the emission color can be further tuned by co-doping with Tb^{3+}. The chromaticity coordinates for the co-doped phosphor, $K_{0.4}Na_{0.6}Sr_{0.995-y}PO_4$:0.005$Eu^{2+}$, y$Tb^{3+}$, can be adjusted from (0.202, 0.406) for $y = 0$ to (0.232, 0.420) for $y = 0.09$. The energy transfer processes from the sensitizer (Eu^{2+}) to the activator (Tb^{3+}) are studied and demonstrated to have a resonance-type dipole–dipole interaction mechanism, with the critical distance of the energy transfer calculated to be 12.46 Å using a concentration quenching method.

Received 21st January 2013
Accepted 21st May 2013

DOI: 10.1039/c3tc30128a

www.rsc.org/MaterialsC

Introduction

The trend towards energy saving technologies in the lighting industry together with regulatory or legal initiatives has put the end of the incandescent lamp in sight and given another push for more widespread use of white light-emitting diodes (WLEDs).[1] WLEDs fabricated with tricolor phosphors and near ultraviolet light-emitting diodes (NUVLEDs) are considered to be very promising for the realization of high-quality light sources because of their higher color rendering index (CRI) and homogeneous color distribution in comparison to current commercial WLEDs.[2] LED phosphors are generally required to have a high conversion efficiency, excellent chemical stability and high thermal quenching temperatures.[1–4] In addition, they are also expected to have a tunable emission color,[4] allowing WLED designers to have greater flexibility in choosing the emission wavelength and gain an improvement either in the correlated color temperature or CRI of WLEDs and for phosphor applications in NUVLEDs.[5]

Recently, $ABPO_4$-type phosphate compounds (where A and B are mono and divalent cations, respectively) acting as host materials for phosphors have drawn an increasing amount of attention due to their excellent thermal, chemical and hydrolytic stabilities.[6,7] Additionally, the variety of the structures in these compounds makes it possible to finely tune the physical/chemical properties to design new materials.[6–8] $KSrPO_4$ is one of the most important members of the phosphate compounds. For example, $KSrPO_4$:Eu^{2+} blue-emitting phosphors show better thermal stability than the currently available YAG phosphor at high temperatures (~225 °C) and are considered to be potential blue-emitting phosphors for WLEDs.[6] More recent works have been done on $KSrPO_4$:Eu^{2+} phosphors, describing both their crystal structure and optical properties.[5,8] However, the emission from these phosphors is too blue (~426 nm) to create a suitable white light. In this paper, we present two strategies for tuning the emission color of a $KSrPO_4$:Eu^{2+} phosphor by: (1) introducing a foreign cation, Na^+, to modify the crystal field strength acting upon the Eu^{2+} activators and (2) introducing a co-doping activator, Tb^{3+}, into the host lattice to promote an energy transfer from Eu^{2+} to Tb^{3+}. The emitting color can be tuned from 426 to 498 nm using strategy (1) and the wavelength can be further extended

[a]Center for Advanced Optoelectronic Functional Materials Research, Key Laboratory for UV-Emitting Materials and Technology of Ministry of Education, Northeast Normal University, 5268 Renmin Street, Changchun 130024, China. E-mail: xtzhang@nenu.edu.cn; Fax: +86 431 85099772; Tel: +86 431 85099772

[b]Department of Physics, Georgia Southern University, Statesboro, GA 30460, USA. E-mail: xwang@georgiasouthern.edu

† Electronic supplementary information (ESI) available. See DOI: 10.1039/c3tc30128a

to 545 nm using strategy (2). The modification of the crystal field is discussed in detail with regard to the crystal structure changes, photoluminescence excitation, lifetime decay, cathodoluminescence (CL) and micro CL mapping. The resonance-type energy transfer from Eu^{2+} to Tb^{3+} ions in the $K_{0.4}Na_{0.6}Sr_{0.995}PO_4$:0.005$Eu^{2+}$, y$Tb^{3+}$ phosphor is demonstrated to have a dipole–dipole interaction mechanism and the crystal distance of the energy transfer is calculated to be 12.64 Å. In short, this $K_{1-x}Na_xSr_{0.995}PO_4$:0.005$Eu^{2+}$, y$Tb^{3+}$ phosphor with a tunable emission color may have potential application in phosphor-converted WLEDs.

Experimental

Samples were synthesized using a conventional solid-state reaction. Stoichiometric amounts of K_2CO_3 (99.99%), Na_2CO_3 (99.95%), Eu_2O_3 (99.99%), NaH_2PO_4 (99.95%) and Tb_4O_7 (99.99%) were ground in an agate mortar. The mixtures were placed in alumina crucibles with covers and were sintered at 1623 K for 3 h by slowly raising the temperature under a reducing CO atmosphere in a muffle furnace. The pellets produced were cooled quickly to room temperature and were ground into powders in an agate mortar. The samples were sintered again at 1623 K under a reducing CO atmosphere in a muffle furnace for 1 h, then cooled to room temperature and ground into powders for subsequent use.

The composition and phase purity of the samples were studied with Cu Kα radiation ($\lambda = 1.5406$ Å) using a Rigaku D/max-2500 X-ray diffractometer (XRD). Photoluminescence (PL) spectra were recorded using a home-made photoluminescence measurement system, which consisted of a NUVLED array (365 nm emission and 14 nm FWHM) as an excitation source, a miniature fiber optic spectrometer (Ocean Optics USB 4000) as a detector, and a glass cell (with an active area of 1.5 × 1.5 cm^2) to contain the pressed powder samples. The lattice constants of the $K_{1-x}Na_xSr_{0.995}PO_4$:0.005$Eu^{2+}$ powders were calculated using the UnitCell program (general cell parameters analysis system). Photoluminescence excitation (PLE) spectra of the powders were recorded using a RF-5301 fluorescence spectrophotometer equipped with a 150 W Xe lamp as an excitation source in the fluorescence mode. The CL and CL mapping measurements were carried out with a field emission scanning electron microscope system (Quanta 250, FEI) equipped with a CL detector (MonoCL 4 system, Gatan). The phosphors were excited by an electron beam under an accelerating voltage of 20 kV and filament currents of 300 μA. All of the CL mapping images were taken in panchromatic mode for investigating the luminescent properties of the phosphor particles. Decay curves for the samples were recorded using an FLS920 fluorescence spectrophotometer (Edinburgh Instruments) with a nanosecond Flashlamp (nF 920) as the light source. The absolute QY was determined using a PL quantum-efficiency measurement system (C9920-02, Hamamatsu Photonics). The QY measurement system was calibrated using rhodamine B, a standard fluorescence solution. All measurements were performed at room temperature.

Results and discussion

Fig. 1a shows the XRD patterns of the (K_{1-x},Na_x)-$Sr_{0.995}PO_4$:0.005Eu^{2+} ($0 \le x \le 0.7$) powders prepared using the solid-state reaction. The $KSr_{0.995}PO_4$:0.005Eu^{2+} powders show the characteristic pattern associated with an orthorhombic structure (space group *Pnma*) and are coincident with JCPDS card no. 33-1045. XRD patterns of the (K_{1-x},Na_x)-$Sr_{0.995}PO_4$:0.005Eu^{2+} ($0 < x \le 0.7$) samples all maintain the features of the orthorhombic structure. However, the diffraction peaks shift slightly to the higher angle side with increasing Na^+ concentration, as shown in Fig. 1b. This observation indicates that substitution of K^+ ($r = 1.37$ Å, CN = 4) with smaller Na^+ ($r = 0.99$ Å, CN = 4) causes a change in the lattice constant of the host lattice, which can be calculated by indexing the XRD data. As shown in Fig. 1c, the lattice constants *a* and *b* decrease linearly as the Na^+ concentration increases, each with a different decay rate, while there is little change in lattice constant *c*. These observations suggest that the introduction of Na^+ shrinks and distorts the $KSrPO_4$ host lattice. The distortion of the host lattice will have a strong impact on the luminescence properties of the Eu^{2+} ions with 5d energy levels, which will be discussed later in the section on photoluminescence. For the Na^+ concentration where $x \ge 0.6$, some unknown byproducts

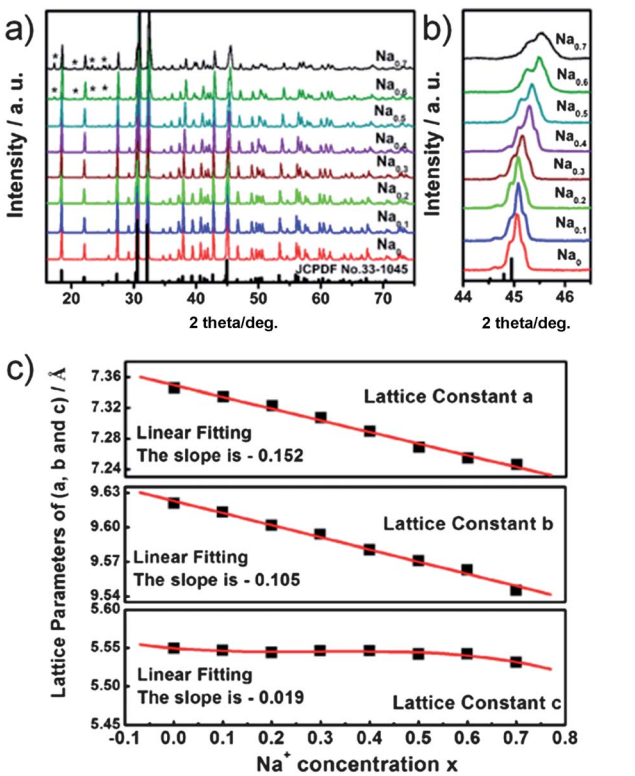

Fig. 1 (a) XRD patterns of the $K_{1-x}Na_xSr_{0.995}PO_4$:0.005$Eu^{2+}$ phosphor as a function of Na^+ concentration. As a reference, the standard XRD data for $KSrPO_4$ is shown. (b) Magnified XRD patterns in the region between 44 and 47 degrees for the $K_{1-x}Na_xSr_{0.995}PO_4$:0.005$Eu^{2+}$ phosphors ($x = 0$, 0.1, 0.2, 0.3, 0.4, 0.5, 0.6, 0.7). (c) Unit cell parameters of the $K_{1-x}Na_xSr_{0.995}PO_4$:0.005$Eu^{2+}$ phosphors ($x = 0$, 0.1, 0.2, 0.3, 0.4, 0.5, 0.6, 0.7) show a contraction in the lattice parameters *a* and *b*, but an almost constant value for lattice parameter *c*.

appear in the powder samples and a heterogeneous mixture of $KSrPO_4$ and $NaSrPO_4$, rather than a uniform solid solution, are observed.

It is usually assumed that Eu^{2+} would take up the Sr site in the $KSrPO_4$ lattice, since there is only one alkaline cation site available. However, Huang *et al.* confirmed that there were three crystallographic cationic sites in the $KSrPO_4$ compound, and that there existed a certain degree of disorder between the potassium and strontium ions.[9,10] In our case, two emission bands centered at 430 and 486 nm are observed under excitation at 365 nm (shown in Fig. 2a) and these are assigned to the $4f^6 5d^1$–$4f^7$ transitions of the Eu^{2+}. This indicates that there are two different Eu^{2+} sites in the $KSrPO_4$ host and thus supports Huang's earlier report. As shown in Fig. S1 (see ESI,†) the emission spectrum can be deconvoluted into two Gaussian components with maxima at 430 (referred to Eu(1)) and 480 nm (referred to as Eu(2)). The probability of the Eu(1) site being occupied dominates over the Eu(2) site, based on the emission intensity. In $KSrPO_4$:Eu^{2+}, the average interatomic distance between Eu^{2+} and oxygen (d_{Eu-O}) is 2.757 Å for an Eu^{2+} occupying a K^+ site and 2.607 Å for a Sr^{2+} site. In general, the bond length affects the crystal field strength significantly. Thus, we infer that the band at 430 nm, assigned to Eu(1), is occupying a K^+ site with a weak crystal field, and the other one at 480 nm, corresponding to Eu(2), is occupying a Sr^{2+} site with a strong crystal field.

Increasing the Na^+ concentration from $x = 0$ to $x = 0.6$ causes the intensity of the higher energy emission band of the Eu(1) site to decline gradually, whereas the intensity of the lower energy band Eu(2) site increases steadily.

We believe that the concentration dependence is due to the preference for Eu^{2+} ions to occupy the Eu(2) site over Eu(1), which has also been observed in other systems.[11] The other possible reason for the concentration dependence is an energy transfer from Eu(1) to Eu(2), however this is not supported by experimental observation. Decay curves of the $K_{1-x}Na_xSrPO_4$:0.005Eu^{2+} (x = 0, 0.1, 0.2, 0.4, 0.5, 0.6, 0.8) phosphors are presented in Fig. S2 (see ESI†) and obtained upon excitation at 390 nm and monitoring the emission peaks located at 430, 434, 437, 440, 444 and 452 nm, respectively. The fluorescence lifetimes of Eu(1) are calculated to be 0.944, 0.942, 1.02, 1.06, 0.91 and 0.87 μs. It is found that lifetimes for the Eu(1) site stay nearly the same with increasing Na^+ ($x < 0.6$) concentration, when taking calculation error into consideration. For higher concentrations of Na^+ ($x > 0.6$), the reduction of the Eu(1) site lifetimes can be attributed to the introduction of an impurity phase. Based on the above results, the enhancement of the Eu(2) site emission is mainly caused by a preference for the Eu(2) site to be occupied. The QY of the $K_{0.4}Na_{0.6}Sr_{0.995}PO_4$:0.005$Eu^{2+}$ phosphor is 50.6% under UV excitation at 385 nm. A further increase in the QY of our samples can be expected by optimizing the preparation conditions.

Additionally, a continuous red shift in the PL spectra is observed with increasing Na^+ concentration. The red shift can be partly ascribed to the changes in the crystal field strength acting upon Eu^{2+}, because incorporation of the Na^+ ions into the lattice causes distortion and changes to the symmetry of the host lattice, as discussed previously, which results in an increase of the crystal field spitting for the 5d energy levels.[12,13] For variations in crystal field strength, one of the phenomenological characteristics is a change in the position and shape of the excitation band.[14,15] As shown in Fig. 2d, with increasing Na^+ concentration, different excitation spectra for the lower energy emission bands testify to an increase of the crystal field strength acting upon Eu^{2+}. Fig. 2b shows the Stokes shift as a function of the Na^+ concentration. It is clearly depicted that the Stokes shift of both emission bands increase as the doped Na^+

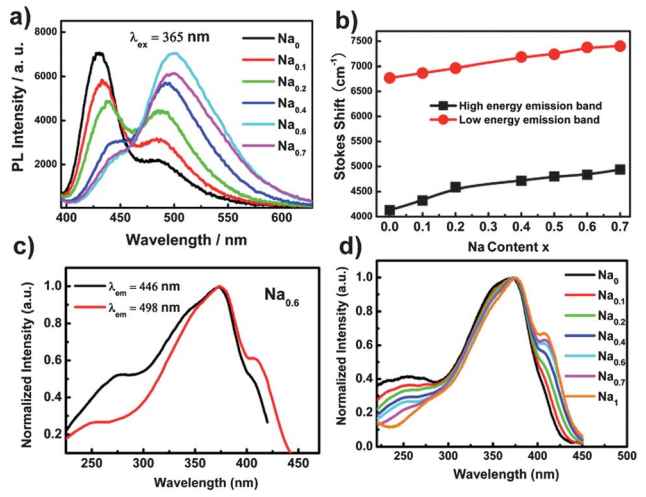

Fig. 2 (a) The PL spectra of the $K_{1-x}Na_xSr_{0.995}PO_4$:0.005$Eu^{2+}$ phosphor as a function of Na^+ concentration under excitation at 365 nm. (b) The variation of the Stokes shift of the two emission bands of the $K_{1-x}Na_xSr_{0.995}PO_4$:0.005$Eu^{2+}$ phosphors (x = 0, 0.1, 0.2, 0.4, 0.6, 0.7). (c) Normalized PLE spectra of the $K_{0.4}Na_{0.6}Sr_{0.995}PO_4$:0.005$Eu^{2+}$ phosphor from monitoring the emission of Eu^{2+} at 446 and 498 nm, respectively. (d) Normalized PLE spectra of the $K_{1-x}Na_xSr_{0.995}PO_4$:0.005$Eu^{2+}$ phosphor as a function of Na^+ concentration obtained by monitoring the low energy emission band of Eu^{2+} (λ_{em} = 498 nm).

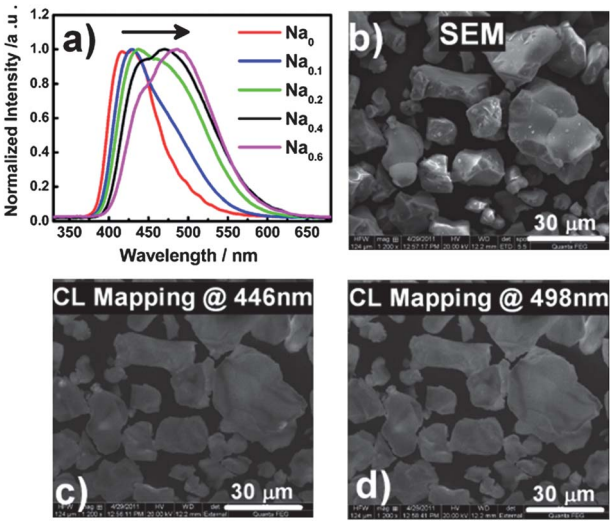

Fig. 3 (a) Normalized CL spectra of the $K_{1-x}Na_xSr_{0.995}PO_4$:0.005$Eu^{2+}$ phosphors (x = 0, 0.1, 0.2, 0.4, 0.6) excited under a low-voltage electron beam. (b) An SEM image of the $K_{0.6}Na_{0.4}Sr_{0.995}PO_4$:0.005$Eu^{2+}$ phosphor. (c) and (d) The monochromatic CL mappings taken at wavelengths of 446 and 498 nm, respectively, for the $K_{0.6}Na_{0.4}Sr_{0.995}PO_4$:0.005$Eu^{2+}$ phosphor.

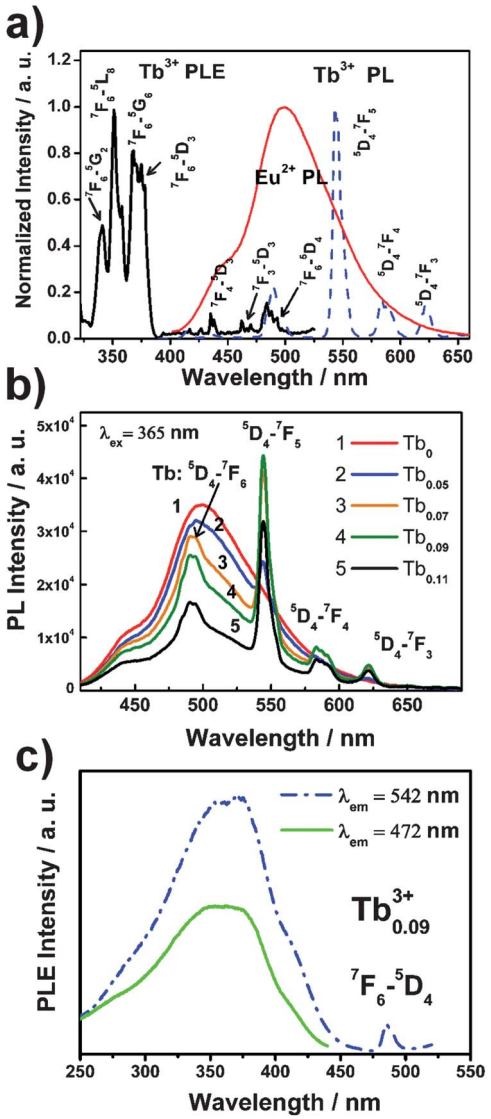

Fig. 4 (a) Spectral overlap between the PL spectrum of a single Eu^{2+}-doped $K_{0.4}Na_{0.6}SrPO_4$ phosphor and the PLE spectrum of a single Tb^{3+}-doped $K_{0.4}Na_{0.6}SrPO_4$ phosphor. In addition, the PL spectrum of a single Tb^{3+}-doped $K_{0.4}Na_{0.6}SrPO_4$ is also shown. (b) PL spectra of the $K_{0.4}Na_{0.6}Sr_{0.995-y}PO_4$:0.005$Eu^{2+}$, yTb^{3+} phosphors (y = 0, 0.05, 0.07, 0.09) under excitation at 365 nm. (c) PLE spectra of the $K_{0.4}Na_{0.6}Sr_{0.995-y}PO_4$:0.005$Eu^{2+}$, yTb^{3+} phosphors (y = 0, 0.05, 0.07, 0.09) obtained by monitoring the emission at 472 and 542 nm, respectively.

concentration increases, suggesting that the observed red shift can be mainly attributed to the increased site distortion and Stokes shift of the Eu^{2+} ions.

Fig. 2c shows the PLE spectra of the $(K_{0.4},Na_{0.6})Sr_{0.995}PO_4$:0.005$Eu^{2+}$ phosphor obtained by monitoring the emissions at 446 and 498 nm, respectively. Both spectra exhibit a broad band emission from 220 to 450 nm, which can be assigned to the 4f–5d transitions of the Eu^{2+} ions. However, their spectral profiles are different, indicating that the two transitions originate from Eu^{2+} ions occupying two different cation sites,[15] Eu(1) and Eu(2), which is in agreement with the PL results. The normalized PLE spectra of the $(K_{1-x},Na_x)Sr_{0.995}PO_4$:0.005$Eu^{2+}$ phosphors (x = 0, 0.1, 0.2, 0.4, 0.6, 0.7, 1) obtained by monitoring the lower energy

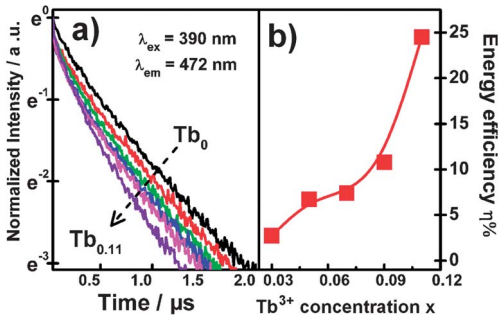

Fig. 5 (a) Luminescence decay curves for Eu^{2+} in the $K_{0.4}Na_{0.6}Sr_{0.995-y}PO_4$:0.005$Eu^{2+}$, yTb^{3+} phosphors (y = 0, 0.03, 0.05, 0.07, 0.09 and 0.11), excited at 390 nm and monitored at 472 nm. (b) The energy transfer efficiency from Eu^{2+} to Tb^{3+} as a function of Tb^{3+} concentration.

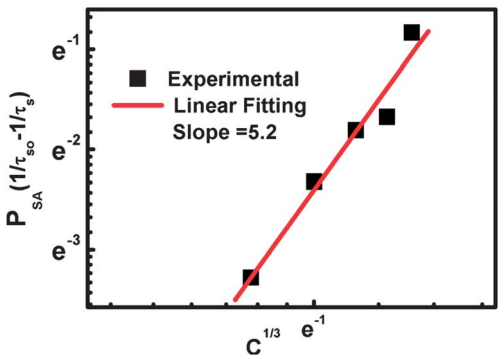

Fig. 6 Dependence of ln(P_{SA}) *versus* ln($C^{1/3}$) for the $K_{0.4}Na_{0.6}Sr_{0.995}PO_4$:0.005$Eu^{2+}$, yTb^{3+} phosphors (y = 0.03, 0.05, 0.07, 0.09 and 0.11). The slope (n = 5.2) indicates that the energy transfer is based on a dipole–dipole interaction.

Table 1 Representation of the CIE chromaticity coordinates of the $K_{1-x}Na_xSr_{0.995-y}PO_4$:0.005$Eu^{2+}$, yTb^{3+} phosphors (λ_{ex} = 365 nm)

No.	$K_{1-x}Na_xSr_{0.995-y}PO_4$:0.005$Eu^{2+}$, yTb^{3+}	CIE (x, y)
1	$x = 0, y = 0$	(0.166, 0.108)
2	$x = 0.2, y = 0$	(0.162, 0.202)
3	$x = 0.4, y = 0$	(0.175, 0.314)
4	$x = 0.6, y = 0$	(0.202, 0.406)
5	$x = 0.6, y = 0.01$	(0.204, 0.415)
6	$x = 0.6, y = 0.03$	(0.212, 0.420)
7	$x = 0.6, y = 0.05$	(0.220,0.425)
8	$x = 0.6, y = 0.07$	(0.230, 0.435)
9	$x = 0.6, y = 0.09$	(0.232, 0.420)

emission bands are shown in Fig. 2d. The onset of the $4f^65d^1$ band in the PLE spectra shifts to the lower energy side as the Na^+ content increases along with profile changes, which are a consequence of the change in the crystal field strength acting upon the Eu^{2+} ions,[16,17] as discussed previously.

The influence of the Na^+-doped concentration on the optical properties of the $KSr_{0.995}PO_4$:0.005Eu^{2+} phosphor is further investigated with CL and micro CL mapping analysis. Fig. 3a depicts the CL spectra of the $(K_{1-x},Na_x)Sr_{0.995}PO_4$:0.005$Eu^{2+}$

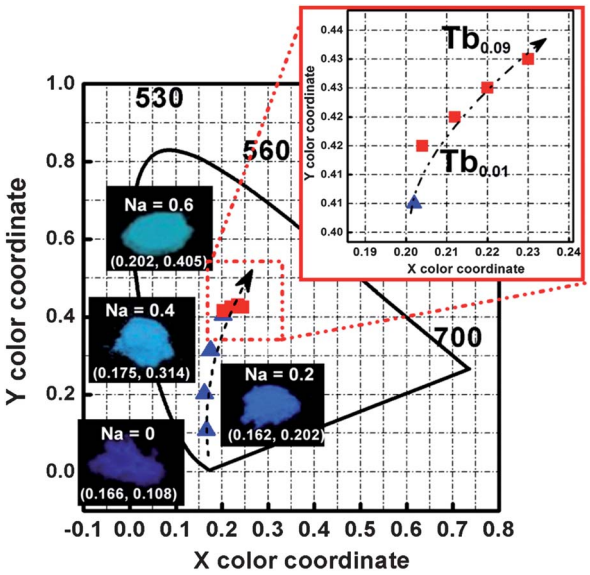

Fig. 7 CIE chromaticity coordinates of the $K_{1-x}Na_xSr_{0.995-y}PO_4$:0.005$Eu^{2+}$ phosphors (x = 0, 0.1, 0.2, 0.4, 0.6, 0.7) under excitation at 365 nm. The insets show digital photos and CIE coordinate values corresponding to selected samples upon excitation with a 365 nm UV lamp. The enlarged area is a representation of the CIE chromaticity coordinates of the $K_{1-x}Na_xSr_{0.995}PO_4$:0.005$Eu^{2+}$, $y$$Tb^{3+}$ phosphors (where y = 0.01, 0.05, 0.07, 0.09) under excitation at 365 nm.

phosphors (x = 0, 0.1, 0.2, 0.4, 0.6). Similar to the PL results, the CL color can also be tuned from deep blue to blue–green by adjusting the Na^+ concentration. Both emission bands, comparable with the PL, become broadened due to the nature of the electronic excitation which has a broad energy distribution. According to the result for the two emission bands of the PL, the monochromatic micro CL mappings of the $(K_{0.4},Na_{0.6})Sr_{0.995}PO_4$:0.005$Eu^{2+}$ phosphor are collected at wavelengths of 446 and 498 nm, from an identical sample position, as shown in Fig. 3c and d. The SEM image of the $(K_{0.4},Na_{0.6})Sr_{0.995}PO_4$:0.005$Eu^{2+}$ phosphor is also presented in Fig. 3b for comparison. Based on the two monochromatic CL mappings, which are recorded from the same scanning area at two different emission wavelengths, a uniform distribution of the Eu^{2+} ions in the phosphor particles can be verified.

Energy transfer plays a very important role in the luminescence properties of a phosphor. Not only can it increase the luminous intensity of a phosphor, but also tune its emission color by varying the relative contents of the sensitizer and activator, such as in the following systems: $Sr_3In(PO_4)_3$:Ce^{3+}/Tb^{3+}/Mn^{2+},[18] $Ca_4Si_2O_7F_2$:Eu^{2+}, Mn^{2+},[19] and $Ca_2Al_3O_6F$:Ce^{3+}, Tb^{3+},[20] $Ca_3Sc_2Si_3O_{12}$:Ce^{3+}, Mn^{2+},[21] $Ca_4Y_6(SiO_4)_6O$:Ce^{3+}/Mn^{2+}/Tb^{3+},[22] and $Ca_9Y(PO_4)_7$:Ce^{3+}, Mn^{2+}.[23] To further tune the emission color in our system, Tb^{3+} is co-doped into the $(K_{0.4},Na_{0.6})Sr_{0.995}PO_4$:0.005$Eu^{2+}$ system as a co-activator. The XRD patterns of the $(K_{0.4},Na_{0.6})Sr_{0.995-y}PO_4$:0.005$Eu^{2+}$, $y$$Tb^{3+}$ phosphor (y = 0, 0.01, 0.03, 0.05, 0.07, 0.09, 0.11) show good agreement with JCPDS card no. 33-1045. However, the diffraction peaks are shift to the high-angle side with increasing Tb^{3+} concentration, suggesting that the Tb^{3+} ions are doped into the host lattice (see Fig. S3 in the ESI†). The PL and PLE spectra of a single Tb^{3+}-doped $(K_{0.4},Na_{0.6})SrPO_4$ sample are shown in Fig. 4a. Under excitation at 365 nm, there is a series of sharp line emissions at 488, 542, 584 and 619 nm, which can be attributed to the characteristic $^5D_4 \rightarrow {}^7F_J$ transitions of Tb^{3+} (where J = 6, 5, 4 and 3, respectively). Monitoring the emission at 542 nm, many sharp peaks are observed within the wavelength range of 300–490 nm in the PLE spectrum, which originated from the intra-4f transitions of Tb^{3+}. For comparison, the PL spectra of a single Eu^{2+}-doped $(K_{0.4},Na_{0.6})SrPO_4$ sample is also shown in Fig. 4a. It can be clearly seen that there is a spectral overlap between the broad emission band of Eu^{2+} and the excitation lines of Tb^{3+} within the spectral range of 400–510 nm. Therefore, a resonance-type energy transfer from Eu^{2+} to Tb^{3+} is expected.[24–26] Fig. 4b gives the PL spectra of selected $(K_{0.4},Na_{0.6})Sr_{0.995-y}PO_4$:0.005$Eu^{2+}$, $y$$Tb^{3+}$ samples (y = 0, 0.05, 0.07, 0.09, 0.11). The luminous intensity of Eu^{2+} at 472 nm (λ_{ex} = 365 nm) decreases steadily with increasing Tb^{3+} concentration, whereas the relative intensity for Tb^{3+} increases initially, before reaching a maximum at y = 0.09. Beyond this the Tb^{3+} intensity decreases slowly, which can be ascribed to Tb^{3+}–Tb^{3+} internal concentration quenching.[20] This result indicates that an energy transfer occurs from Eu^{2+} to Tb^{3+}, which can be further confirmed from the PLE spectra, which is shown in Fig. 4c. Compared with the PLE spectra of a single Eu^{2+}-doped $(K_{0.4},Na_{0.6})SrPO_4$ sample (λ_{em} = 472 nm), the appearance of a broad band transition from Eu^{2+} in the PLE spectra, obtained by monitoring at 542 nm (Tb^{3+} emission), indicates the occurrence of an energy transfer from Eu^{2+} to Tb^{3+}. The emission color of $(K_{0.4},Na_{0.6})Sr_{0.995-y}PO_4$:0.005$Eu^{2+}$, $y$$Tb^{3+}$ phosphors is then tuned by adjusting the Tb^{3+} concentration, as expected.

In order to further investigate the dynamic luminescence process between Eu^{2+} and Tb^{3+}, the PL decay curves of Eu^{2+} in the phosphors were measured, as shown in Fig. 5a. The fluorescence of Eu^{2+} decays faster and tends to be a non-exponential function with increasing the Tb^{3+} concentration. The decay process of these samples are characterized by an average lifetime, τ, which can be calculated using eqn (1) as follows,[26–28]

$$\tau = \frac{\int_0^\infty I(t)t\mathrm{d}t}{\int_0^\infty I(t)\mathrm{d}t}, \quad (1)$$

where $I(t)$ is the luminous intensity at time t. Based on eqn (1), the luminescence lifetimes of Eu^{2+} are determined to be 0.74, 0.72, 0.69, 0.66, 0.65 and 0.56 μs for Tb^{3+} concentrations of 0, 0.03, 0.05, 0.07, 0.09 and 0.11, respectively. The decrease in the lifetimes of Eu^{2+} with increasing Tb^{3+} concentration, strongly demonstrates an energy transfer from $Eu^{2+} \rightarrow Tb^{3+}$. In addition, the energy transfer efficiency (η) from Eu^{2+} to Tb^{3+} is calculated by the following expression:[27,28]

$$\eta = 1 - \tau_s/\tau_{so} \quad (2)$$

where τ_{so} and τ_s represent the lifetime of Eu^{2+} in the absence and the presence of Tb^{3+}, respectively. As shown in Fig. 5b, the energy transfer efficiency increases gradually with increasing

Tb^{3+} concentration. The energy transfer, η, is calculated to be 0%, 2.7%, 6.7%, 7.4%, 10.8% and 24.5% for the $(K_{0.4},Na_{0.6})Sr_{0.995-y}PO_4$:0.005$Eu^{2+}$, yTb^{3+} phosphors with $y = 0$, 0.03, 0.05, 0.07, 0.09 and 0.11, respectively.

In general, energy transfer from the sensitizer to activator in a phosphor may take place *via* a multipolar interaction[29] or an exchange interaction at higher concentrations. On the basis of Dexter's energy transfer expression for multipolar interactions and Reisfeld's approximation,[27,28] the following relationship can be given:

$$P_{SA} = \frac{1}{\tau_{so}} - \frac{1}{\tau_s} \propto C^{n/3} \quad (3)$$

where P_{SA} is the energy transfer probability and C is the concentration of Tb^{3+}. The relationships of $P_{SA} \propto C^{n/3}$ where $n =$ 6, 8 and 10 correspond to dipole–diople, dipole–quadrupole and quadrupole–quadrupole interactions,[29] respectively. Fig. 6 shows the double logarithm plots of P_{SA} *versus* $C^{1/3}$ for the $K_{0.4}Na_{0.6}Sr_{0.995}PO_4$:0.005$Eu^{2+}$, yTb^{3+} phosphors ($y = 0.03$, 0.05, 0.07, 0.09 and 0.11) with a slope $n = 5.2$. The value is close to 6, indicating that the dominant energy transfer mechanism in the phosphor system is a dipole–dipole interaction. The lifetime decay curves in Fig. 5 are not a perfect single exponential, which yields errors when calculating the decay rates when using the average values. On the other hand, the non-exponential decays suggest the involvement of exchange interactions in the energy transfer. Therefore, both factors cause the value of n to be less than 6, which is within experimental error.

The critical distance for the $Eu^{2+} \rightarrow Tb^{3+}$ energy transfer, R_{Eu-Tb}, is calculated using the concentration quenching method suggested by Blasse.[30] R_{Eu-Tb} can be estimated in terms of the equation $R_{Eu-Tb} = 2(3V/4\pi XN)^{1/3}$ (where X denotes the combined concentration of Eu^{2+} and Tb^{3+}; N denotes the number of host cations in the unit cell, and V the volume of unit cell).[25] For the $K_{0.4}Na_{0.6}SrPO_4$ host, $V = 384.87$ Å^3, $N = 4$, and $X = 0.09$. Accordingly, the critical transfer distance for Eu^{2+} and Tb^{3+} in $K_{0.4}Na_{0.6}SrPO_4$ materials is calculated to be 12.46 Å.

The x and y values of the CIE chromaticity coordinates for the selected $(K_{1-x},Na_x)Sr_{0.995}PO_4$:0.005$Eu^{2+}$, yTb^{3+} phosphors are calculated and presented in Table 1 and Fig. 7. As shown, the chromaticity coordinates can be tuned from deep blue (0.166, 0.108) to blue–green (0.210, 0.276) by adjusting the Na^+ concentration. The insets in Fig. 7 show digital photographs corresponding to $x = 0$, 0.2, 0.4 and 0.6 under a 365 nm UV lamp. Fig. 7 demonstrates the color tuning to blue–green (0.210, 0.276) by adjustment of the Na^+ concentration. The enlarged area shown in Fig. 7 shows the tuning range of the chromaticity coordinates of the $(K_{0.4},Na_{0.6})Sr_{0.995}PO_4$:0.005$Eu^{2+}$, yTb^{3+} phosphors changing from (0.202, 0.406) for $y = 0$ to (0.232, 0.420) for $y = 0.09$.

Conclusions

In summary, we have synthesized two series of $K_{1-x}Na_xSr_{0.995}PO_4$:0.005$Eu^{2+}$ and $K_{0.4}Na_{0.6}Sr_{0.995-y}PO_4$:0.005$Eu^{2+}$, yTb^{3+} phosphors *via* a high-temperature solid-state reaction and investigated their luminescence properties and crystal structures. Their emission colors are tunable by modulating the crystal field strength and energy transfer. Replacing part of the host lattice cation K^+ with Na^+ causes a contraction and distortion of the unit cell and lowers the symmetry of the host lattice, such that the emitting color can be tuned from deep blue (~426 nm) to blue–green (~498 nm). The red-shifted emission is due to the increased crystal field splitting of Eu^{2+} at a lowered symmetry site. The emission color can be further tuned using energy transfer by co-doping Tb^{3+} into the system and the chromaticity coordinates of the $K_{0.4}Na_{0.6}Sr_{0.995}PO_4$:0.005$Eu^{2+}$, yTb^{3+} phosphors can be adjusted from (0.202, 0.406) for $y = 0$ to (0.240, 0.420) for $y = 0.09$. Energy transfer from Eu^{2+} to Tb^{3+} is demonstrated to have a resonance-type dipole–dipole interaction mechanism, with the critical distance of the energy transfer calculated to be 12.46 Å. $K_{0.4}Na_{0.6}Sr_{0.995}PO_4$:0.005$Eu^{2+}$ and $K_{0.4}Na_{0.6}Sr_{0.995-y}PO_4$:0.005$Eu^{2+}$, yTb^{3+} phosphors are promising candidates for application in solid-state lighting or field emission displays.

Acknowledgements

The work is supported by the National Natural Science Foundation of China (Grant no. 51072032, 41001258), the Program for New Century Excellent Talents in University (NECT-10-0320), the National Basic Research Program (2012CB933703), the Fundamental Research Funds for the Central Universities (Grant no. 12QNJJ007, 12SSXM001), and 111 project (no. B13013).

Notes and references

1 P. Hartmann, P. Pachler, E. L. Payrer and S. Tasch, *Proc. SPIE*, 2009, **7231**, 72310X.
2 T. Taguchi, *IEEJ Trans. Electr. Electron. Eng.*, 2008, **3**, 21.
3 X. F. Li, J. D. Budai, F. Liu, J. Y. Howe, J. H. Zhang, X. J. Wang, Z. J. Gu, C. J. Sun, R. S. Meltzer and Z. W. Pan, *Light: Sci. Appl.*, 2013, **2**, 2047.
4 P. F. Smet, A. Parmentier and D. Poelman, *J. Electrochem. Soc.*, 2011, **158**(6), R37–R54.
5 M. Hannah, A. B. Piquette, M. Anc, J. Kittrick, J. Talbot, J. K. Han and K. Mishra, *ECS Trans.*, 2012, **41**, 19.
6 Y. S. Tang, S. F. Hu, C. C. Lin, N. Bagkar and R.-S. Liu, *Appl. Phys. Lett.*, 2007, **90**, 151108.
7 T. S. Chan, R. S. Liu and I. Baginskiy, *Chem. Mater.*, 2008, **20**, 1215.
8 C. C. Lin, Z. R. Xiao, G. Y. Guo, T. S. Chan and R. S. Liu, *J. Am. Chem. Soc.*, 2010, **132**, 3020.
9 S. Y. Zhang, Y. L. Huang and H. J. Seo, *J. Electrochem. Soc.*, 2010, **157**, J261.
10 Y. L. Huang, W. F. Kai, Y. G. Cao, K. W. Jang, H. S. Lee, L. Kim and E. Cho, *J. Appl. Phys.*, 2008, **103**, 053501.
11 S. Ye, J. H. Zhang, X. Zhang, S. Z. Lu, X. G. Ren and X. J. Wang, *J. Appl. Phys.*, 2007, **101**, 033513.
12 G. Blasse and B. C. Grabmaier, *Luminescent Materials*, Springer-Verlag, Berlin, German, 1994, p. 45.
13 C. Ronda, *Luminescent*, Wiley-VCH, Weinheim, 2007, p. 27.
14 H. A. Hope, H. Lutz, P. Morys, W. Schnick and A. Seilmeier, *J. Phys. Chem. Solids*, 2001, **61**, 2001–2006.
15 R. J. Xie, N. Hirosaki, T. Suehiro, F. F. Xu and M. Mitomo, *Chem. Mater.*, 2006, **18**, 5578.

16 S. Y. Zhang and Y. L. Huang, *J. Am. Ceram. Soc.*, 2011, **94**, 2987.
17 K. Denault, N. George, S. Paden, S. Brinkley, A. Mikhailovsky, J. Neuefeind, S. Denbaars and R. Seshdri, *J. Mater. Chem.*, 2012, **22**, 18204.
18 D. L. Geng, G. G. Li, M. M. Shang, D. M. Yang, Y. Zhang, Z. Y. Cheng and J. Lin, *J. Mater. Chem.*, 2012, **22**, 14262.
19 C. H. Huang, T. S. Chan, W. R. Liu, D. Y. Wang, Y. C. Chiu, Y. T. Yeh and T. M. Chen, *J. Mater. Chem.*, 2012, **22**, 20210.
20 Z. G. Xia and R. S. Liu, *J. Phys. Chem. C*, 2012, **116**, 15604.
21 Y. F. Liu, X. Zhang, Z. D. Hao, X. J. Wang and J. H. Zhang, *Chem. Commun.*, 2011, **47**, 10677.
22 G. G. Li, Y. Zhang, D. L. Geng, M. M. Shang, C. Peng, Z. Y. Cheng and J. Lin, *ACS Appl. Mater. Interfaces*, 2012, **4**, 296.
23 C. H. Huang, T.-W. Kuo and T. M. Chen, *ACS Appl. Mater. Interfaces*, 2010, **2**(5), 1395.
24 Y. Chen, J. Wang, X. G. Zhang, G. G. Zhang, M. L. Gong and Q. Su, *Sens. Actuators, B*, 2010, **148**, 259.
25 W. Lu, Z. D. Hao, X. Zhang, Y. S. Luo, X. J. Wang and J. H. Zhang, *Inorg. Chem.*, 2011, **50**, 7846.
26 N. Guo, Y. H. Song, H. P. You, G. Jia, M. Yang, K. Liu, Y. H. Zheng, Y. J. Huang and H. J. Zhang, *Eur. J. Inorg. Chem.*, 2010, 4636.
27 F. Lahoz, I. R. Martín, J. Méndez-Ramos and P. Núñez, *J. Chem. Phys.*, 2004, **120**, 6180.
28 G. Blasse, *Phys. Lett. A*, 1968, 28.
29 G. Blasse and B. C. Grabmaier, *Luminescent Materials*, Springer-Verlag, Berlin, German, 1994, p. 91.
30 G. Blasse, *Phys. Lett.*, 1968, **28**, 6.

